Complex excitability and "flipping" of granule cells: an experimental and computational study

Joanna Danielewicz, Guillaume Girier, Anton Chizhov, Mathieu Desroches, Juan Manuel Encinas, Serafim Rodrigues

▶ **To cite this version:**

Joanna Danielewicz, Guillaume Girier, Anton Chizhov, Mathieu Desroches, Juan Manuel Encinas, et al.. Complex excitability and "flipping" of granule cells: an experimental and computational study. 2023. hal-04232000

HAL Id: hal-04232000
https://hal.science/hal-04232000v1

Preprint submitted on 7 Oct 2023

HAL is a multi-disciplinary open access archive for the deposit and dissemination of scientific research documents, whether they are published or not. The documents may come from teaching and research institutions in France or abroad, or from public or private research centers.

L'archive ouverte pluridisciplinaire **HAL**, est destinée au dépôt et à la diffusion de documents scientifiques de niveau recherche, publiés ou non, émanant des établissements d'enseignement et de recherche français ou étrangers, des laboratoires publics ou privés.

Complex excitability and "flipping" of granule cells: an experimental and computational study

Joanna Danielewicz[1,2], Guillaume Girier[2], Anton Chizhov[3,4], Mathieu Desroches[3,4], Juan-Manuel Encinas[1,5,6†], Serafim Rodrigues[2,6‡]

1 Achucarro Basque Center for Neuroscience, Leioa, Bizkaia, Spain
2 BCAM Basque Center for Applied Mathematics, Bilbao, Bizkaia, Spain
3 Inria Center at Université Côte d'Azur, Sophia Antipolis, France
4 Université Côte d'Azur, Nice, France
5 University of the Basque Country (UPV/EHU), Leioa, Bizkaia, Spain
6 Ikerbasque, The Basque Science Foundation, Bilbao, Bizkaia, Spain

† JM.Encinas@achucarro.org; ‡ srodrigues@bcamath.org

Abstract

In response to prolonged depolarizing current steps, different classes of neurons display specific firing characteristics (i.e. excitability class), such as a regular train of action potentials with more or less adaptation, delayed responses, or bursting. In general, one or more specific ionic transmembrane currents underlie the different firing patterns. Here we sought to investigate the influence of artificial sodium-like (Na channels) and slow potassium-like (KM channels) voltage-gated channels conductances on firing patterns and transition to depolarization block (DB) in Dentate Gyrus granule cells with dynamic clamp - a computer-controlled real-time closed-loop electrophysiological technique, which allows to couple mathematical models simulated in a computer with biological cells. Our findings indicate that the addition of extra Na/KM channels significantly affects the firing rate of low frequency cells, but not in high frequency cells. Moreover, we have observed that 44 percent of recorded cells exhibited what we have called a "flipping" behavior. This means that these cells were able to overcome the DB and generate trains of action potentials at higher current injections steps. We have develop a unified mathematical model of flipping cells to explain this phenomenon. Based on our computational model, we conclude that the appearance of flipping is linked to the number of states for the sodium channel of the model.

Author summary

Managing the diversity of neurons is a very complex yet very important task. Electrophysiological criteria, such as firing characteristics, are commonly used to identify different types of neurons in different brain regions that are sharing anatomical and functional similarities. The main focus of our studies is to explore firing patterns and the transition to depolarization block of granule cells in the Dentate Gyrus, a very important brain region that is the input gate to the mammalian hippocampal formation and has been implicated in spatial navigation, response decorrelation, pattern separation and memory formation. Based on our electrophysiological recordings, specifically on the firing rates, we describe two subpopulations within granule cells, low- and high frequency neurons. However, the major finding of this study is the discovery of a new

electrophysiological phenomenon that we call “flipping”. This neuronal behavior, which we recorded with the use of dynamic-clamp technique, has not been reported in other experimental studies. Our description and our computational model of the “flipping” phenomenon gives more insights into electrophysiological behavior of granule cells.

Introduction

Depolarization block - a silent state that occurs when a neuron receives excessive excitation - is a very important feature and is regarded to have pathological relevance for some brain disorders, including epilepsy and schizophrenia [1–3]. Furthermore, depolarization block in dopaminergic neurons was suggested to explain the therapeutic action of antipsychotic drugs [3]. Among all the mechanisms responsible for transition into depolarization block, the inactivation of voltage-gated sodium channels is believed to play a key role [4–6]. Subsequently, it has been shown that decreasing the sodium conductance pharmacologically causes dopamine neurons to go into DB with lower maximal frequencies at lower values of applied current, whereas augmenting this conductance with the dynamic clamp has the opposite effect [6, 7]. Dynamic clamp, a term for the various combinations of software and hardware that simulate these conductances, has proven to be a valuable tool for electrophysiologists for studying different excitability classes of cells [8].

The dentate gyrus (DG) is the input gate to the mammalian hippocampal formation and has been implicated in spatial navigation, response decorrelation, pattern separation and engram formation. Continual neurogenesis in the adult dentate gyrus produces new granule cells (GCs) that integrate into the hippocampal circuit by establishing synapses with existing neurons [9–12]. Granule cells are the prominent neuronal subtype within the DG, and have been studied extensively from the perspective of their intrinsic response properties. GCs are characterized by their peculiar delayed and heterogeneous maturation. Most of them (85%) are generated postnatally. From the primary dentate matrix, neural precursors migrate to the dentate gyrus between embryonic day 10 and 14 where they differentiate into neurons [13, 14]. Neurogenesis reaches a peak at the end of the first postnatal week and is largely completed toward the end of the first postnatal month [15]. Interestingly, the dentate gyrus retains the capability to give rise to new neurons throughout life, although at a reduced rate [16, 17]. In adulthood, after being generated in the subgranular zone, immature GCs are incorporated into pre-existing circuits, thus contributing to improve several brain functions including learning and memory processes. During a transient period of maturation, new GCs exhibit intrinsic and synaptic properties distinct from mature GCs, potentially underlying the contribution of neurogenesis to memory encoding [12, 18–23].

The vast repertoire of electrical activity displayed by neurons is the result of membrane-bound ion channels, each producing a distinct conductance that facilitates current flux through the membrane. These conductances may be static, or their magnitudes may be voltage- or ligand-dependent. The intrinsic firing properties and ionic conductances in GCs are thought to reflect their developmental stage and maturation level [18, 24, 25]. Among DG granule cells, input resistance (R_i), threshold current (I_{thr}), and firing patterns have been used as signatures of the degree of maturation and circuitry integration. During the first few days, postmitotic neurons remain in the proliferative subgranular zone and display very high input resistance (several gigaohms), because of the low density of K+ channels in the plasma membrane. Immature GCs also express voltage-dependent Na- and K-channels at a low density. Thus, depolarizing current steps elicit ”immature” action potential (single spikes with small amplitude and long duration) in current-clamp recordings [16, 17, 26]. Maturating GCs show a progressive decrease in input resistance and an increase in spike amplitude

and frequency, suggesting that a deep rearrangement of voltage-operated and non-gated channels occurs at the same time.

In this study, we focused on exploring firing patterns and the transition to depolarization block of granule cells in the dentate gyrus by using dynamic clamp electrophysiological recordings. We applied dynamic clamp recordings to explore the diversity of neurons and to tackle their excitability by adding artificial sodium-like or potassium-like voltage-gated channels. This approach allowed us to describe for the first time a new electrophysiological phenomenon that we have called "flipping".

Materials and methods

Animals and treatment

Four- to six-week old C57BL/6 mice were used for all procedures. Mice were housed at constant humidity and temperature with a 12-h light/dark cycle with food ad libitum. The use of animals for experimentation and the experimental procedures are included in the approved protocols M20_2022_129 (2022-2025); M20_2022_130 (2022-2025) that have been reviewed and approved by the ethics (CEID and CEIAB) committees of the UPV/EHU and the Diputación Foral de Bizkaia.

Preparation of brain slices

Mice were anestethized with isoflurane and decapitated. Their brains were quickly removed and placed in ice-cold artificial cerebrospinal fluid (ACSF) containing (in mM): 92 NMDG, 2.5 KCl, 0.5 $CaCl_2$, 10 $MgSO_4$, 1.25 NaH_2PO_4, 30 $NaHCO_3$, 20 HEPES, 5 Na-ascorbate, 3 Na-pyruvate, 2 Thiourea and 25 D-glucose (pH 7.3 – 7.4; 300 – 310 mOsm) and bubbled with the mixture of 95% O2 – 5% CO2. Coronal slices (thickness = 250 µm) containing DG were cut from hemisphere ipsilateral to the TBI/Sham surgery using a vibrating microtome (Leica VT1000). Slices were stored submerged in room temperature for recovery.

Electrophysiology

After 1-1.5 h individual slices were placed in the recording chamber mounted on the stage of Scientifica microscope with 40x water immersion lens and superfused at 3 ml/min with warm (32 ± 0.5 °C), modified ACSF of the following composition (in mM): 124 NaCl, 4.5 KCl, 1.25 NaH_2PO_4, 26 $NaHCO_3$, 1 $MgSO_4$ * 7 H_2O, 1.8 $CaCl_2$, and 10 D-glucose (pH 7.3-7.4; 300-310 mOsm), bubbled with the mixture of 95% O2 – 5% CO2. Recording micropipettes were pulled from borosilicate glass capillaries (Science Products) using the PC-100 Nareshige puller. The pipette solution contained (in mM): 125 K-gluconate, 20 KCl, 2 $MgCl_2$, 10 HEPES, 4 Na_2-ATP, 0.4 Na-GTP, 5 EGTA (pH 7.3-7.4; 295-305 mOsm,). Pipettes had open tip resistances of approx. 7-9 MΩ. The calculated liquid junction potential using this solution was 13.1 mV, and data were corrected for this offset. Signals were recorded using Axon MultiClamp 700B amplifier (Molecular Devices), filtered at 2 kHz, and digitized at 20 kHz using Digidata 1550A (Molecular Devices) interface and Clampex 10 software (Molecular Devices, USA).

Cell access was obtained in the voltage-clamp mode and Resting Membrane Potential (RMP) was measured immediately upon break-in in the current-clamp mode by setting the clamp current equal to zero. In order to understand better the functional role of ion channels in shaping the electrical activity and entry to depolarization block granule cells were recorded under dynamic clamp conditions. In our specific setup, a second computer was connected to the MultiClamp 700B amplifier via the NI DAQ

PCI-6221-37pin (National Instruments, Austin, TX). We employed a dynamic-clamp setup with open source software[1]. Contrary to alternative available dynamic clamp distributions, our software allows for a flexible development environment, which is the key requirement for later enhancements of specific experimental protocols. Once the two systems were connected, whole-cell recordings were performed in real-time, currents injected into the cell were directly dependent on measured voltage. The firing characteristics of the recorded cells was assessed using intracellular injections of rectangular current pulses of increasing amplitude (range:- 200 pA to + 1200 pA; duration: 500 ms) and f-I curves (firing rate vs injected current) were constructed. With dynamic clamp, we mimicked additional channels and assessed several parameters, like conductance, half-maximum location of the activation and inactivation functions of the ion channels responsible for general electrical activity and entry to DB of the recorded cells. To describe the additional currents, we employed conventional approximations such as Hodgkin-Huxley ones for potassium channels, and Markovian model for sodium channels. Only cells with stable access resistance were accepted for the data analysis. A schematic of our experimental set up is presented in Fig. 1.

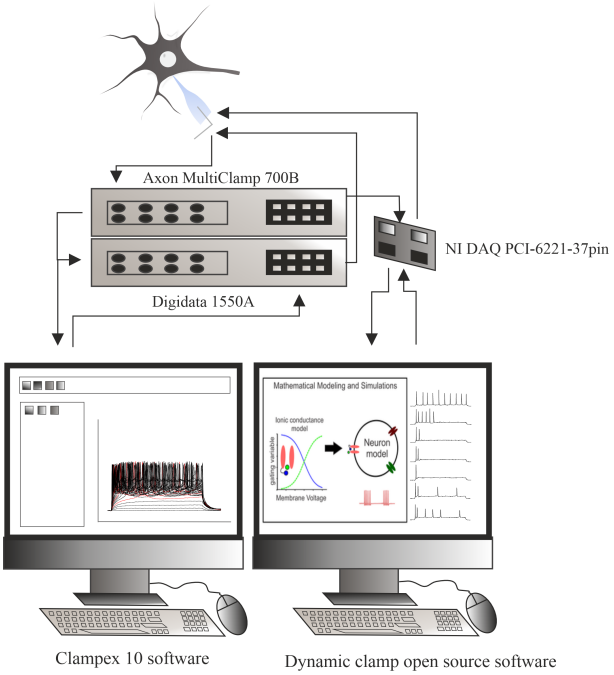

Fig 1. Dynamic-clamp experimental setup

In the experiments where additional shunting was mimicked, the injected current was calculated as a linear function of V:

$$I_{\text{inj}}(V,t) = u(t) - s(t)(V + 60\,\text{mV}), \tag{1}$$

where $u(t)$ and $s(t)$ are step functions of time. The reference membrane potential was choosen to be equal to -60mV.

In the experiments with the additional sodium and potassium channels, the injected current was as follows:

$$I_{\text{inj}}(V,t) = I_{\text{Na}}(V) + I_{\text{K}}(V) + I_{\text{KM}}(V) + u(t) - s(t)(V + 60\,\text{mV}), \tag{2}$$

where I_{Na}, I_{K} and I_{KM} were calculated according to ODEs coming from a mathematical model.

[1]Available at http://www.ioffe.ru/CompPhysLab/AntonV3.html

Statistical analysis

Statistical analysis was performed using the dynamic clamp open source software Visualizator[2] and GraphPad Prism[3]. Data were analyzed using a one–way ANOVA. Post hoc analysis for ANOVA was conducted by using Tukey's test. The level of statistical significance was set at $p < 0.05$. All data sets were tested for deviation from normal distribution (Kolmogorov–Smirnov's test).

Computational Modelling

We have combined multi-timescale mathematical modelling for excitability framework developed in our previous work [27] and conductance-based modelling.

The model's equations are defined as follows:

$$C\frac{dV}{dt} = g_L(V - V_L) - I_{Na} - I_{DR} - I_A + u(t) - s(t)(V - V_{us}) \tag{3}$$

Approximating formulas for the currents I_{Na}, I_{DR} and I_A are taken from [28]. The voltage-dependent potassium current I_{DR} is defined as :

$$I_{DR}(V) = \bar{g}_{DR} n y_K (V - V_K), \tag{4}$$

$$\frac{dn}{dt} = \frac{n_\infty(V) - n}{\tau_n(V)}, \tag{5}$$

$$\frac{dy_K}{dt} = \frac{y_{K\infty}(V) - y_K}{\tau_y(V)}, \tag{6}$$

$$\begin{aligned} \tau_n &= \frac{1}{\alpha_n + \beta_n} + 0.8\,\text{ms}, \quad n_\infty = \frac{\alpha_n}{\alpha_n + \beta_n} \\ \alpha_n &= 0.17 \cdot \mathrm{e}^{(V+5)\cdot 0.090}\,\text{ms}^{-1}, \quad \beta_n = 0.17 \cdot \mathrm{e}^{(V+5)\cdot 0.022}\,\text{ms}^{-1}, \\ \tau_y &= 300\,\text{ms}, \quad y_{K\infty} = \frac{1}{1 + \mathrm{e}^{(V+68)\cdot 0.038}} \end{aligned} \tag{7}$$

The voltage-dependent potassium current I_A is defined as :

$$I_A(V) = \bar{g}_A n_A^4 l_A^3 (V - V_K), \tag{8}$$

$$\frac{dn_A}{dt} = \frac{n_{A\infty}(V) - n_A}{\tau_n(V)}, \tag{9}$$

$$\frac{dl_A}{dt} = \frac{l_{A\infty}(V) - l_A}{\tau_l(V)}, \tag{10}$$

$$\begin{aligned} \tau_{n_A} &= \frac{1}{\alpha_{n_A} + \beta_{n_A}} + 1\,\text{ms}, \quad n_{A\infty} = \frac{\alpha_{n_A}}{\alpha_{n_A} + \beta_{n_A}} \\ \alpha_{n_A} &= 0.08 \cdot \mathrm{e}^{(V+41)\cdot 0.089}\,\text{ms}^{-1}, \quad \beta_{n_A} = 0.08 \cdot \mathrm{e}^{(V+41)\cdot 0.016}\,\text{ms}^{-1}, \\ \tau_{l_A} &= \frac{1}{\alpha_{l_A} + \beta_{l_A}} + 2\,\text{ms}, \quad l_{A\infty} = \frac{\alpha_{l_A}}{\alpha_{l_A} + \beta_{l_A}}, \\ \alpha_{l_A} &= 0.04 \cdot \mathrm{e}^{-(V+49)\cdot 0.11}\,\text{ms}^{-1}, \quad \beta_{l_A} = 0.04\,\text{ms}^{-1}, \end{aligned} \tag{11}$$

[2]Available at http://www.ioffe.ru/CompPhysLab/AntonV3.html
[3]https://www.graphpad.com/

The voltage-dependent sodium current I_{Na} was approximated by the following 4-state Markov model [28]:

$$I_{Na}(V) = \bar{g}_{Na} x_1 (V - V_{Na}), \tag{12}$$

$$x_1 + x_2 + x_3 + x_4 = 1, \tag{13}$$

$$\frac{dx_i}{dt} = \sum_{j=0, j\neq 1}^{4} A_{j,i} x_j - x_i \sum_{j=0, j\neq 1}^{4} A_{i,j} \text{ with } i = 1, 2, 3, \tag{14}$$

$$\begin{aligned} &A_{1,2} = 3 \text{ ms }, A_{1,3} = f_1^{1,3}(V), A_{1,4} = f_1^{1,4}(V), \\ &A_{2,1} = 0, A_{2,3} = f_2^{2,3}(V), A_{2,4} = 0, \\ &A_{3,1} = f_1^{3,1}(V), A_{3,2} = 0, A_{3,4} = f_2^{3,4}(V), \\ &A_{4,1} = f_1^{4,1}(V), A_{4,2} = 0, A_{4,3} = 0, \end{aligned} \tag{15}$$

$$\begin{aligned} f_1^{i,j}(V) &= \left\{ \tau_{min}^{i,j} + \frac{1}{\mathrm{e}^{(V - V_{1/2}^{i,j})/k^{i,j}}} \right\}^{-1} \\ f_2^{i,j}(V) &= \{ \tau_{min}^{i,j} + [(\tau_{max}^{i,j} - \tau_{min}^{i,j})^{-1} + \mathrm{e}^{(V - V_{1/2}^{i,j})/k^{i,j}}]^{-1} \}^{-1}, \end{aligned} \tag{16}$$

Results

Intrinsic properties, firing pattern and depolarization block

We studied the firing patterns and the capabilities of granule cells for entering DB under dynamic clamp conditions. Firing rate was assessed by constructing f-I curves for each individual neuron; see Fig. 2 B. Furthermore, the maximum frequency of generating action potentials was calculated as the number of spikes per stimulation time (500 ms). Because DB depends not only on the injected current but also on the extra (synaptic) conductance (additional shunting), we measured the dependence of firing rate versus current and conductance (Fig. 2A), thus revealing the full domain of spiking in the plane of those input parameters, which can be re-interpreted in terms of excitation and inhibition in the following way:

$$I_{\text{inj}}(V, t) = v(t) - s(t)(V + 60\,\text{mV}) = G_{\text{E}}(t)(V_{\text{E}} - V) + G_{\text{I}}(t)(V_{\text{I}} - V), \tag{17}$$

that is,

$$u(t) = G_{\text{E}}(t)(V_E + 60\text{mV}) + G_{\text{I}}(t)(V_I + 60\,\text{mV}), \quad s(t) = G_{\text{E}}(t) + G_{\text{I}}(t), \tag{18}$$

where G_{E} and G_{I} are the excitatory and inhibitory synaptic conductances, respectively.

Entrance into DB was defined when the recorded cells started generating action potentials with half of the maximum spiking frequency, and the u_{DB}/G_{in} parameter was measured, where u_{DB} is the value of u that leads to DB, and G_{in} is the input conductance of neuron at the resting state, evaluated from responses to current step injection. Based on firing characteristics, specifically maximum frequency of generating action potentials, we have observed that recorded cells can be divided into two main groups:

1) LFC (low-frequency cells) generating action potentials with a maximum frequency lower than 12 Hz (9 cells out of 18; Fig. 3 A,C), and

2) HFC (high-frequency cells) generating action potentials with a frequency higher that 12 Hz (9 out of 18 cells; Fig. 3B,C).

The maximum spiking frequency reached by LFC cells was significantly lower when compared to HFC cells (7.5 ± 1.4 Hz vs 22.9 ± 2.1 Hz, $p < 0.0001$; see Fig. 3 D).

In LFC cells, the firing rate decreased for u_{DB}/G_{in} bigger then 56.4 ± 6.38 mV due to depolarization block and it was siginificantly lower than for HFC cells (79 ± 10 mV; $p < 0.05; F = 2.5; t = 1.9; df = 14$; see Fig. 3 E), which indicates that LFC neurons are entering into DB earlier than HFC cells. We have compared basic intrinsic properties of recorded LFC and HFC cells, such as action potential (AP) amplitude, resting membrane potential (RMP), the duration of action potential measured as AP half width, input resistance, threshold for generating AP and tau. There were no significant differences between two groups (see Table 1). Therefore, we suggest that the maximum firing rates of different neurons are mainly related to the current critical for entering DB.

	RMP (mV)	AP Amplitude (mV)	AP Half width (ms)	Treshold (mV)	R_i (MΩ)	Tau (ms)	n
LFC	-75,84±2,429	128,5±2,712	1,287±0,135	-37,78±3,401	284,1±27,54^{ns}	16,91±1,56	9
HFC	-76,26±0,847	131,9±1,525	1,101±0,038	-42,18±2,222	205,7±21,58	18,59±2,39	9

Table 1. Basic parameters of recorded neurons. Data presented as $mean \pm SEM$; there were no significant differences between the groups ($p > 0.05$ ANOVA). LFC - low frequency cells, HFC - high frequency cells, RMP - resting membrane potential, R_i - input resistance, n - number of recorded cells.

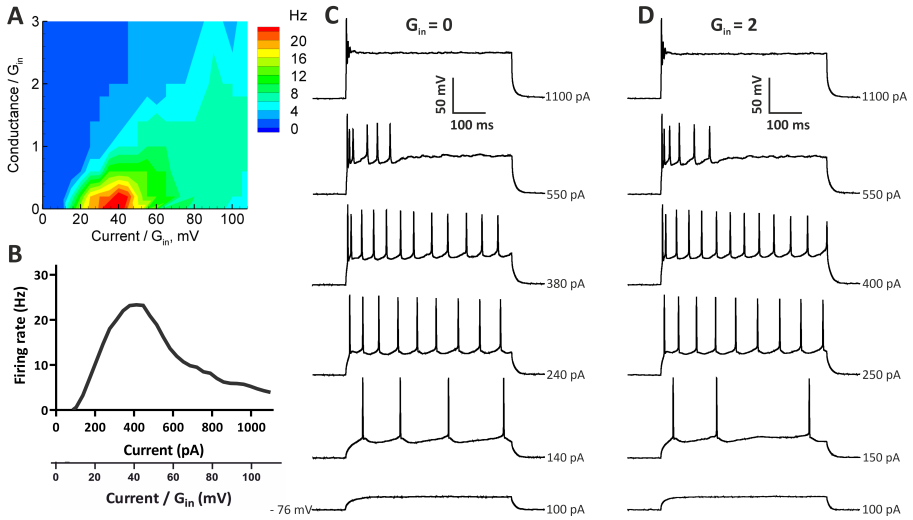

Fig 2. Assesment of firing rate in examplary neurons. (A) Firing rate as the number of APs per stimulation time interval (500ms) for a representative neuron as a function of injected current u and extra conductance s, both scaled by the input conductance G_{in}=9.9nS. Cell 21/C4. (B) Firing rate vs injected current steps (f-I curve) for cell 21/C4. (C) Representative responses of 21/C4 cell to sub- and suprathreshold depolarizing current pulses showing spiking pattern, entrance to DB and full depolarization block without extra conductane (G_{in}=0). (D) Representative responses of 21/C4 cell to sub- and suprathreshold depolarizing current pulses showing spiking pattern, entrance to DB and full depolarization block under shunting conditions (G_{in}=2)

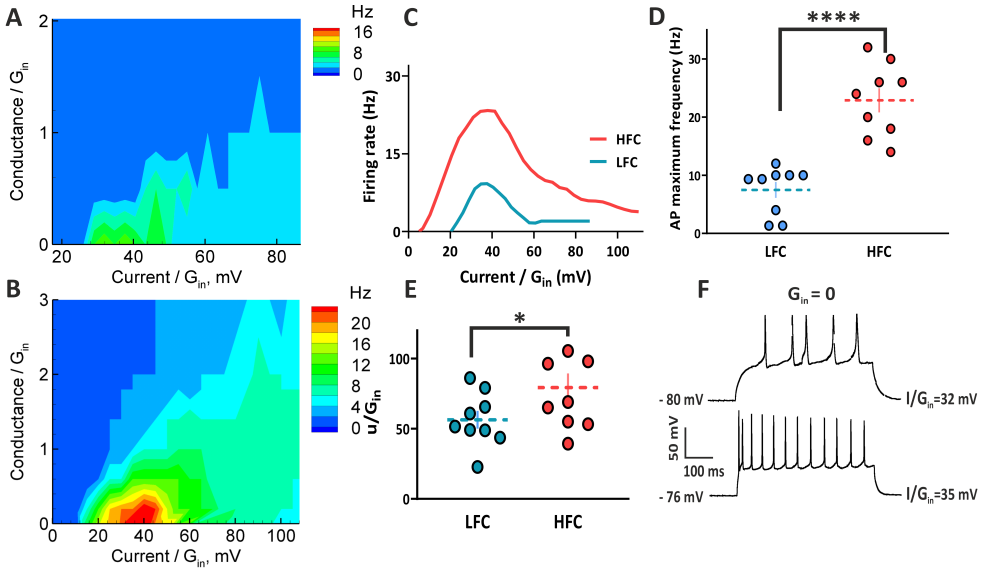

Fig 3. Comparison between two subpopulations of recorded cells. (A) Firing rate for a representative LFC neuron as a function of injected current and extra conductance, both scaled by the input conductance G_{in}=3.5nS. Cell 21/C1. (B) Firing rate for a representative HFC neuron as a function of injected current and extra conductance, both scaled by the input conductance G_{in}=9.9nS. Cell 21/C4. (C) f-I curves for representative LFC and HFC cells. (D) Maximum spiking frequency in LFC neurons was significantly lower than in HFC neurons. (E) LFC neurons are entering depolarization block earlier than HFC neurons. (F) Representative responses of LFC (top) and HFC (bottom) cells to suprathreshold depolarizing current pulse. Data presented as $mean \pm SEM$ (Horizontal dashed line); **** indicate statistical significance $p < 0.0001$ ANOVA; * indicate statistical significance $p < 0.05$ ANOVA

Effect of extra channels

We studied whether additional sodium and potassium channels would significantly affect both firing rates and entrance into the depolarization block of recorded granule cells. We implemented the addition of both sodium and potassium channels and assuming that the maximum firing rate is controlled by the currents that provide spike frequency adaptation, we decided to add slow potassium channels (KM-channels). As a result, LFC neurons started showing much higher values of firing rate and the maximum frequency of generating action potentials was significantly higher when additional Na/KM channels were introduced (without extra channels 7.5 ± 1.4 Hz vs with Na/KM channels 36 ± 3 Hz; $p < 0.0001$; $F = 4.5$; $t = 8$; $df = 8$; Fig. 4 A,C). However, adding Na/KM channels did not significantly affected the u_{DB}/G_{in} parameter, therefore the entrance into DB of LFC cells has not been influenced (without extra channels 56 ± 6 mV vs with Na/KM channels 54 ± 9 mV; $p = 0.4$; $F = 1.6$; $t = 0.17$; $df = 11$; Fig. 4 D). In the HFC group, after adding extra Na/KM channels, a change to f-I curve previously observed in the LFC neurons was present only in 1 out of 9 recorded cells. In remaining HFC neurons additional Na/KM channels did not affected firing rate (Fig. 4 B,C). Overall, the mean maximum frequency of generating action potentials in HFC cells was not significantly altered by the addition of Na/KM channels (without extra channels 23 ± 2 Hz vs with Na/KM channels 36 ± 13 Hz; $p = 0.34$; $F = 30$; $t = 1.0$; $df = 7.5$; Fig. 4 B,C). In HFC group, after adding Na/KM channels, cells tend to enter DB block earlier than without additional channels as the value of the u_{DB}/G_{in} parameter is

smaller, however this shift is not statistically significant (without extra channels 82 ± 11 mV vs with Na/KM channels 66 ± 18 mV; $p = 0.23$; $F = 2.3$; $t = 0.76$; $df = 10$; Fig. 4 D).

While analyzing f-I curves plots of recorded neurons we have observed an interesting phenomenon regarding depolarization block. In several granule cells, after adding Na/KM channels we observed a complex, non-gradual dependence of firing rate on injected current.

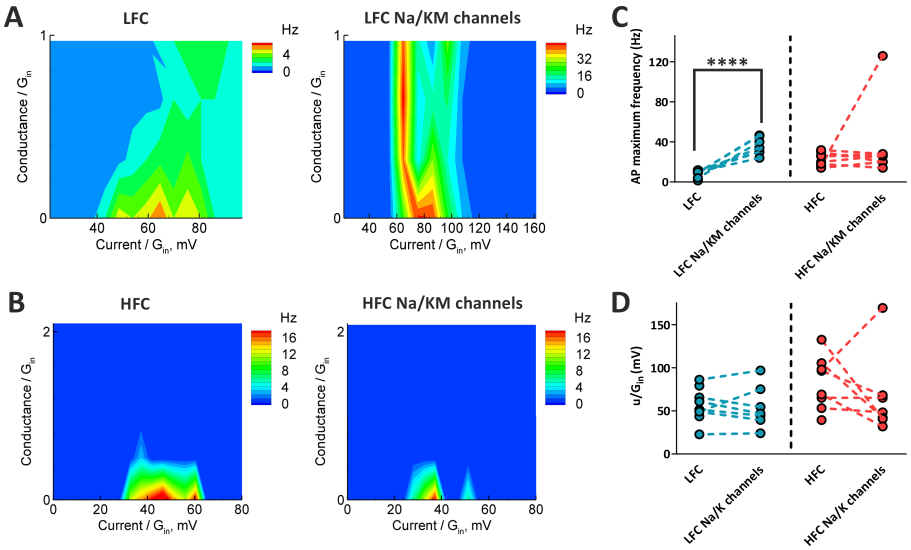

Fig 4. Effects of additional sodium and slow potassium channels on firing rate and enterance to depolarization block. (A) Firing rate for a representative LFC neuron without (left) and with additional Na/KM channels (right; g_{Na}=200 nS, g_{KM}=200 nS). (B) Firing rate for a representative HFC neuron without (left) and with additional Na/KM channels (right; g_{Na}=10 nS, g_{KM}=10 nS). (C) Maximum spiking frequency was significantly increased in LFC neurons, but not in HFC cells. (D) Addition of Na/KM channels does not influence the u/G_{in} parameter. Data presented as $mean \pm SEM$; **** indicate statistical significance $p < 0.0001$ ANOVA.

"Flipping" cells

While, in general, the initial entrance into DB was not affected by additional Na/KM channels as there were no significant differences in u_{DB}/G_{in} parameter (as described in the previous section), 8 out of 18 recorded neurons expressed a very unique behavior in terms of their firing patterns. After reaching a full DB characterized as generating only 1 or 2 action potentials in response to injected current step, these cells were not able to maintain it, instead they "flipped" and started generating trains of spikes at larger injected current steps before finally reaching another DB. We called this phenomenon "flipping" (Fig. 5). Interestingly, even within this small subpopulation of "flipping" cells we were able to observe two different types of "flipping" behavior. Half of the recorded cells were able to overcome the DB only once, meaning one big "flip" was present in their firing responses to current injection. However, the remaining half of the "flipping" neurons were able to produce multiple "flips" (2 to 8). In general, we observed that the majority (5 out of 8) of "flipping" neurons were previously assigned to the LFC group and within this subpopulation 2 cells were able to generate multiple "flips" (2 and 3 flips). The remaining 3 "flipping" cells were HFC neurons and 2 of those cells were able to generate 6 and 8 "flips" in response to injected current step (Fig. 6 A). As the

majority of “flipping” cells generating only one ”flip” were previously assigned to the LFC group, we wondered whether the number of ”flips” is correlated with the initial spiking frequency. We have observed a positive correlation between the number of ”flips” and the maximum frequency of action potentials generated by the cell in control conditions, meaning without additional Na/KM channels ($r = 0.74$; $R^2 = 0.54$; $p = 0.037$; Fig. 6 F), however there was no correlation between the number of generated ”flips” and the maximum spiking frequency recorded with additional Na/KM channels present ($r = 0.24$; $R^2 = 0.055$; $p = 0.58$; Fig. 6 G). Because “flipping” is a phenomenon that we have never come across before, we wondered what could be the possible mechanism behind it, for this purpose we designed and analysed a computational model.

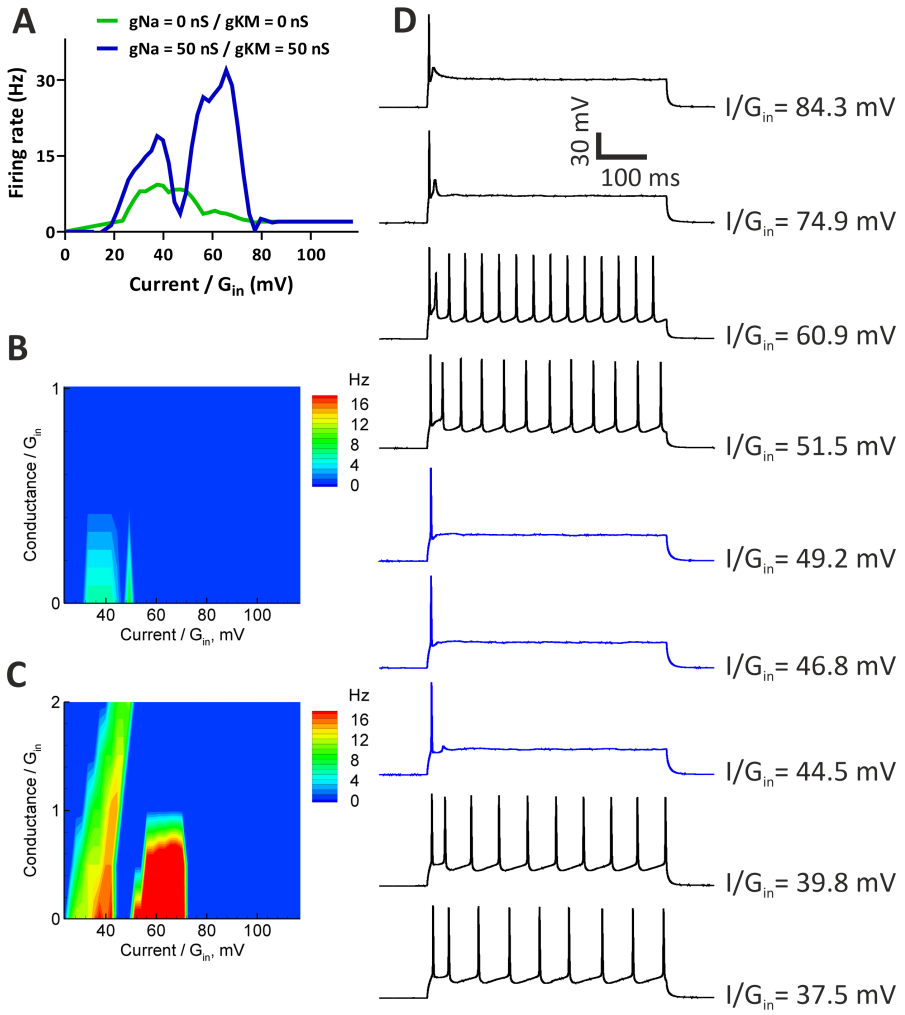

Fig 5. Example of the “flipping” phenomenon. (A) f-I curves of a representative cell exhibitng a pronounced ”flip” in firing pattern induced by the addition of g_{Na}=50 nS, g_{KM}=50 nS channels (blue line). (B, C) Firing rate as a function of injected current and extra conductance, both scaled by the input conductance G_{in}=4.27nS without (B) and with (C) additional Na/KM channels. (D) Representative responses to a suprathreshold depolarizing current pulses.

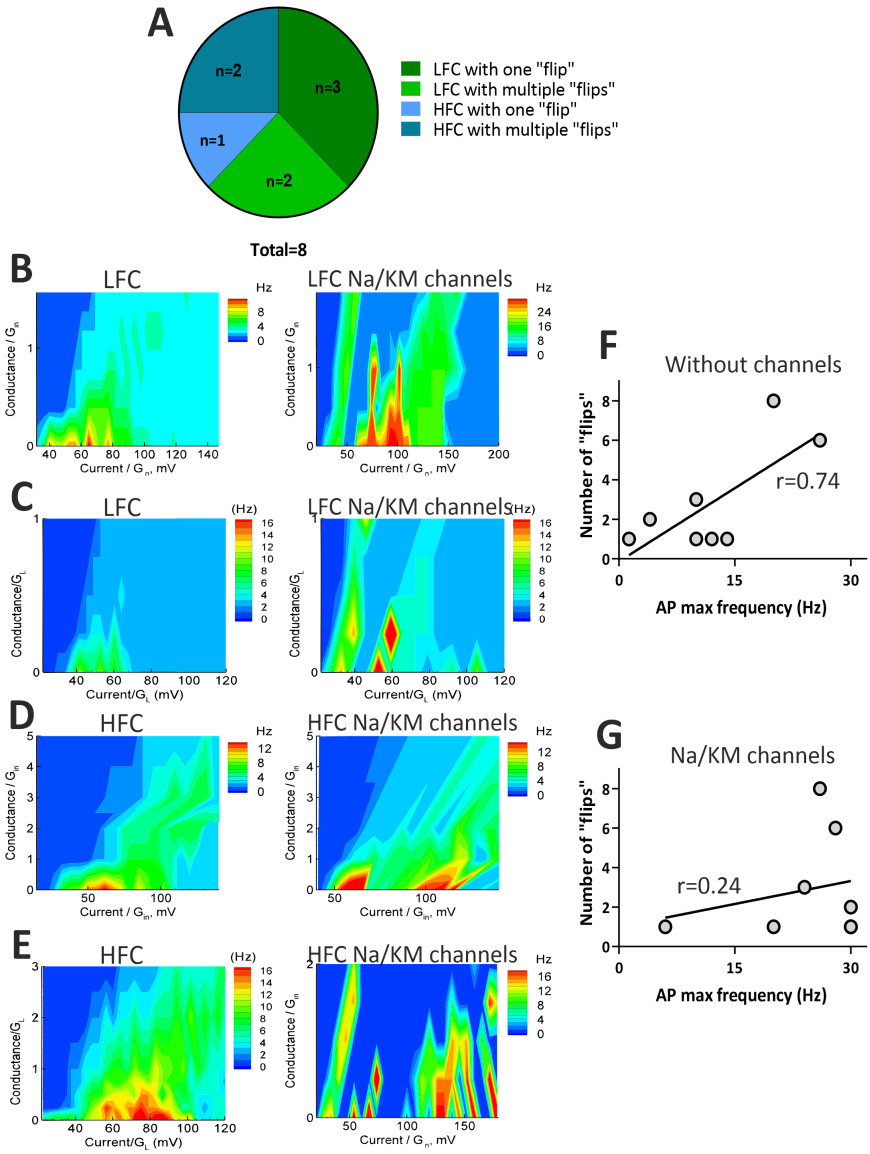

Fig 6. "flipping" cells. (A) Division of "flipping" cells based on the number of "flips" and the initial firing rate (LFC vs HFC). (B) Firing rate of a LFC neuron generating one "flip" after addition of g_{Na}=100 nS, g_{KM}=40 nS; Cell 21/C3. (C) Firing rate of a LFC neuron generating multiple "flips" after addition of g_{Na}=50 nS, g_{KM}=50 nS; Cell 21/C6. (D) Firing rate of a HFC neuron generating one "flip" after addition of g_{Na}=50 nS, g_{KM}=20 nS; Cell 21/C2. (E) Firing rate of a HFC neuron generating multiple "flips" after addition of g_{Na}=50 nS, g_{KM}=50 nS; Cell 21/C7. (F) The number of "flips" is correlated with the maximum frequency of spikes generated in response to injected current step before the addition of Na/KM channels. (G) The number of "flips" is not correlated with the maximum frequency of spikes generated in response to injected current step after the addition of Na/KM channels.

"Flipping" in a computational model

In order to analyze the "flipping" effect, we simulated a neuron with a Na- and K-channels. In the present model, the "flipping" is observed only for nonzero extra

conductance. The excitation domain (Fig. 7 A) has a "horn" on the right. Hence, the f-I curve shows a gap (Fig. 7 C), which is due to the "flipping". In terms of spike trains (Fig. 7 B), this gap is revealed as a cease of spiking for intermediate currents, and constant spiking in response to smaller and larger currents. At large currents, however, the amplitude of spikes is different, which is explained by a different sequence of transitions undergone by the sodium channels between the states of the Markov model. While during weak stimulus the hyperpolarization between spikes is stronger and the channels pass through low- and high-threshold states, for larger current the neuronal membrane is always depolarised between spikes and the channels pass only through high-threshold states. This recruitment of different channel states in different regimes causes the "flipping" behavior.

Blockade of potassium channels in the model leads to shrinkage of the excitation domain (Fig. 7 D), but remains the split and thus "flipping".

In the reduced model with only Na-channels present, the "flipping" is observed in wider range of extra conductances.

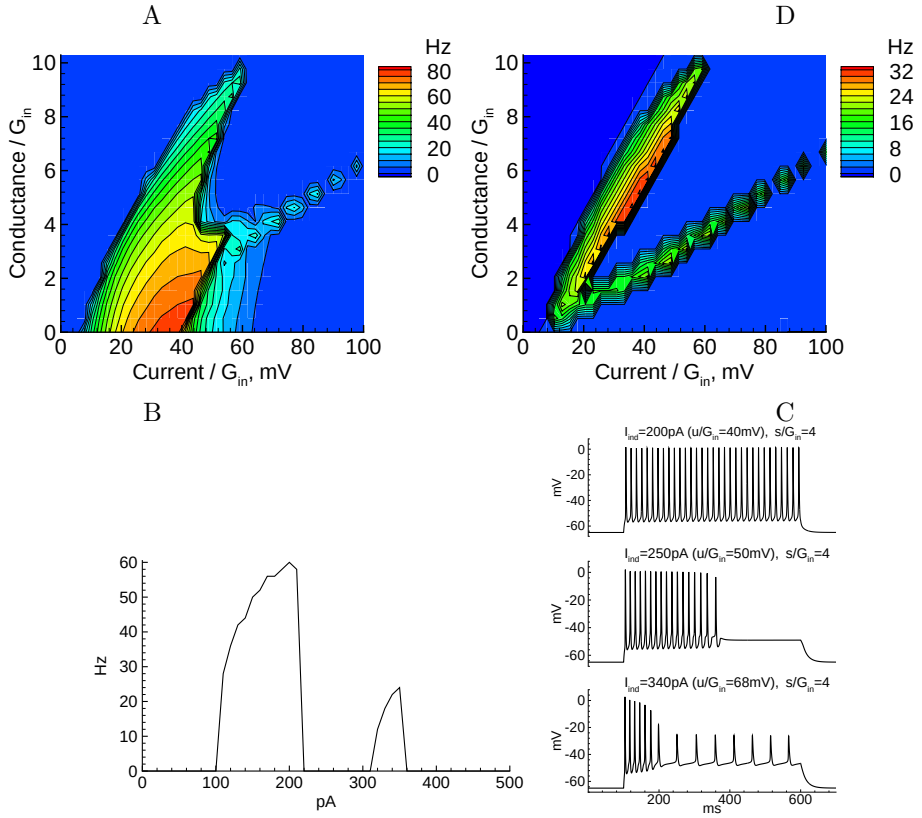

Fig 7. Simulations of a neuron with Na- and K-channels. g_{Na}=228nS, g_{KM}=500nS, G_{in}=5nS. A: f-u-s dependence; B: f-I curves for s/G_{in}=4; C: spike trains. D: Reduced model with only Na-channels.

Bifurcation analysis of "flipping"

With the model introduced above, it is possible to reproduce the phenomenon of "flipping", and its appearance is linked to the number of states for the sodium channel of the model. With three states for this channel, the model displays one periodic regime upon variations of the applied current, and this regime is bounded in parameter space

by Hopf bifurcations (one supercritical and one subcritical); see Fig 8. Namely, a family

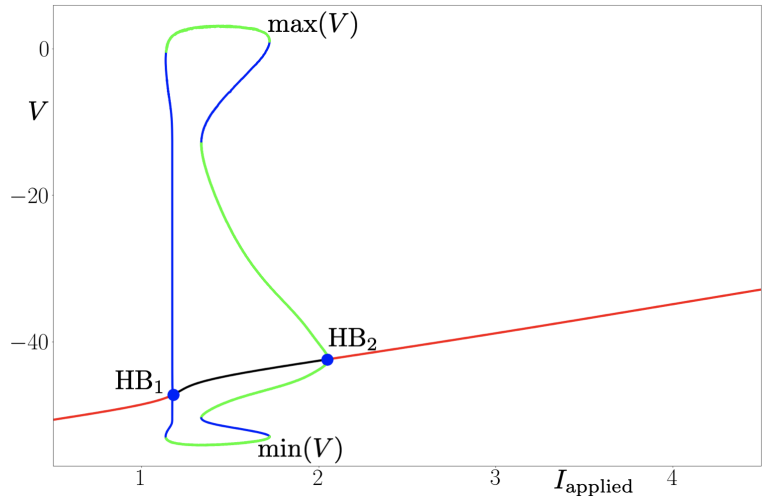

Fig 8. Bifurcation diagram of the system with 3 states, and with respect to parameter I_{applied}. Red (resp. black) segments of the curve of equilibria denote stable (resp. unstable) branches. As the applied current I_{applied} is increased, oscillations (spikes) appear through a supercritical Hopf (HB_1) and then disappear through a subcritical Hopf bifurcation (HB_2). Parameter values are: $\tau_{min}^{1,3} = 0.33$ ms, $\tau_{min}^{3,1} = 0.33$ ms, $\tau_{min}^{2,3} = 1.0$ ms, $V_{\text{half}}^{1,3} = -51$mV, $V_{\text{half}}^{3,1} = -42$mV,$V_{\text{half}}^{1,3} = -53$mV, $k^{1,3} = -2,0$ mV, $k^{3,1} = 1,0$ mV, $k^{2,3} = -1,0$ mV, $\tau_{max}^{2,3} = 100$ ms, $V_{Na} = 65$ mV, $V_K = -70$ mV, $V_L = -64.96$ mV, $\bar{g}_{Na} = 2.28\mu S/cm^2$S, $\bar{g}_{DR} = 0.76\mu S/cm^2$, $\bar{g}_A = 8.36\mu S/cm^2$, $\bar{g}_L = 0.048\mu S/cm^2$, $s = 0.2cm^2$, $V_{us} = -49$ mV, $C = 0.7\mu$F/cm^2, $A^{1,2} = 3$ ms^{-1}. Initial conditions are : $V_0 = -65$, $x_1 = 0$, $x_2 = 0$, $n_0 = 0.00128$, $y_{K,0} = 0.47$, $n_{A,0} = 0.079$, $l_{A,0} = 0.85$.

of low-voltage equilibria (rest states of the neuron) destabilise and give way to a family of stable limit cycles (spiking states of the neuron) via a supercritical Hopf bifurcation (HB_1), which occurs at an input current value $I \approx 1.2$. At a much higher value of the input current, the branch of stable cycles disappears via a subcritical Hopf bifurcation (HB_2) at $I \approx 2$. This scenario is compatible with type-2 neural excitability.

In contrast, when the number of states is increased to four, the two Hopf bifurcations from the previous scenario are still present, for similar values of applied current (HB_1, HB_2), however a second periodic regime appears, bounded in parameter space by a second pair of Hopf bifurcations, at higher values of $I_{applied}$; see Fig 9. Indeed, at an input current value $I \approx 3.2$, the stable solution destabilise again and give way to a family of stable limit cycles via a supercritical Hopf (HB_3). This branch of stable cycles disappears via a subcritical Hopf bifurcation (HB_4) at $I \approx 4.1$. The two pairs of Hopf bifurcations are separated by a regime where the model admits a stable stationary state with voltage higher than the firing threshold, hence a DB. Therefore, this second periodic regime arising at larger values of the input current is therefore compatible with the "flipping" phenomenon reported in the present work, and it is due to the number of sodium channel states in the model.

Discussion

Managing the diversity of neurons is a very complex yet very important task. Electrophysiological criteria, such as intrinsic properties, excitability class represented

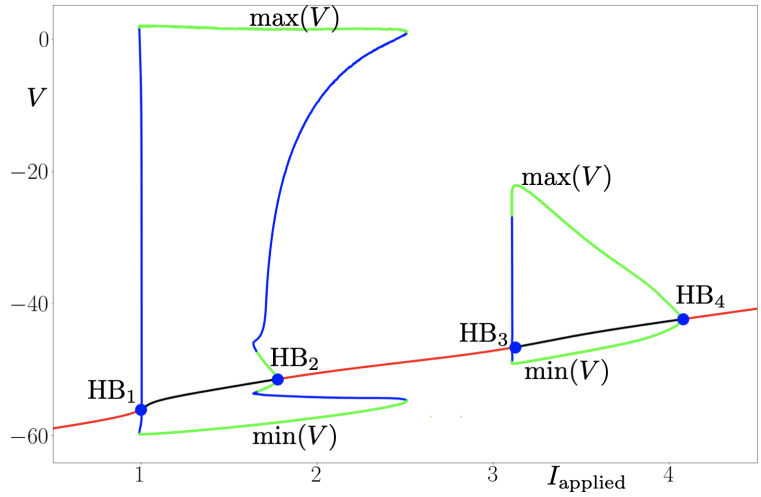

Fig 9. Bifurcation diagram of the system with 4 states, and with respect to parameter I_{applied}. Red (resp. black) segments of the curve of equilibria denote stable (resp. unstable) branches. As the applied current I_{applied} is increased, oscillations (spikes) appear through a supercritical Hopf (HB_1) and then disappear through a subcritical Hopf bifurcation (HB_2). Then, the scenario appears for higher values of I_{applied} : oscillations appear through a subcritical Hopf (HB_3) and then disappear through a supercritical Hopf (HB_4) Parameter values are: $\tau_{min}^{1,3} = 0.33$ ms, $\tau_{min}^{3,1} = 0.33$ ms, $\tau_{min}^{2,3} = 1$ ms, $\tau_{min}^{1,4} = 0.33$ ms, $\tau_{min}^{3,4} = 1ms$, $\tau_{min}^{4,1} = 0.33$ ms, $V_{\text{half}}^{1,3} = -51$mV, $V_{\text{half}}^{3,1} = -57$mV,$V_{\text{half}}^{1,3} = -53$mV, $V_{\text{half}}^{1,4} = -57$mV, $V_{\text{half}}^{3,4} = -60$mV, $V_{\text{half}}^{4,1} = -51$mV, $k^{1,3} = -2$ mV, $k^{3,1} = 1$ mV, $k^{2,3} = -1$ mV, $k^{1,4} = -2$ mV, $k^{3,4} = -1$ mV, $k^{4,1} = 1,0$ mV, $\tau_{max}^{2,3} = 100$ ms, $\tau_{max}^{3,4} = 100$ ms, $V_{Na} = 65$ mV, $V_K = -70$ mV, $V_L = -64.96$ mV, $\bar{g}_{Na} = 2.28\mu S/cm^2$, $\bar{g}_{DR} = 0.76\mu S/cm^2$, $\bar{g}_A = 8.36\mu S/cm^2$, $\bar{g}_L = 0.048\mu S/cm^2$, $s = 0.2cm^2$, $V_{us} = -49$ mV, $C = 0.7\mu$F/cm^2, $A^{1,2} = 3$ ms^{-1}. Initial conditions are : $V_0 = -65$, $x_1 = 0$, $x_2 = 0$, $n_0 = 0.00128$, $y_{K,0} = 0.47$, $n_{A,0} = 0.079$, $l_{A,0} = 0.85$.

by firing patterns and transition to depolarization block are very useful tools in identifying and distinguishing different types of neurons that are sharing anatomical and functional similarities. Therefore, the primary goal of this study was to explore firing characteristics and entrance into depolarization block of granule cells.

Depolarization block of granule cells is very rarely discussed in experimental findings probably because the range of input currents in which GCs transition to DB could be considered unphysiological, especially in the case of mature GCs. However, a model developed for hippocampal CA1 region by Bianchi suggests that even background synaptic activity in the gamma range involving less than 3 percent of the total number of excitatory synaptic inputs converging on any given CA1 pyramidal neuron, could easily generate an aggregate peak input current larger than 1 nA [4]. This finding makes the DB a very important feature of any neuron, because it is highly probable that in large active networks, such as dentate gyrus, numerous cells will likely be in a DB at any time, therefore their silent state could influence the activity of the entire network.

Many studies focusing on the excitability of granule cells reported two main types of firing patterns that GCs generate in response to increasing current injections. Typically, type-1 DG granule cells are exhibiting spikes starting from a moderate intensity of stimulation and increasing in frequency following steps increments. At current injections of high intensity, these cells are lacking sustained firing, action potentials become progressively smaller in amplitude and GCs are entering DB at a relatively early stage (200-250 pA). In contrast, type-2 DG granule cells are usually described as firing

throughout all the current step without failure (entering DB) and exhibiting firing frequencies that were linearly proportional to the intensity of the current step, i.e. the maximum number of action potentials was always observed for the highest current intensity [29–31]. Based on results obtained in our study, we observed that LFC neurons resemble the type-1 cells reported by others. In our experimental protocol, however, we used a wider range of current intensities therefore we were able to observe the transition of HFC (type-2) GCs into DB at a later stage (450-500 pA). That approach, with applying current intensities greater than 300 pA, is not typically used by others, therefore only linear firing patterns of type-2 GCs is most commonly described in other experimental findings.

Under physiological conditions, neurons fire in response to the activation of synaptic conductances. In electrophysiological experiments, usually, neuronal characteristics are probed in current-clamp conditions, which cannot fully reflect the synaptic activation because the injected current cannot mimick changes of membrane conductance, if only it is not voltage-dependent. The conductance change provides shunting effect, whose importance is shown, for instance, in visual cortex studies [32, 33]. Such characteristics of neuronal activity as the firing rate and the spike shape parameters are much more fully expressed by their dependence on both signals, the synaptic current and synaptic conductance, or, the injected voltage-independent current and conductance [34, 35]. These signals determine the first two, voltage-independent and linearly voltage-dependent components of the total current received by a neuron from synaptic input [34]. Therefore, in our study we used the dynamic-clamp technique, because it can provide both input signals, the synaptic current and the synaptic conductance [36, 37]. The dynamic-clamp stimulation protocols used in our study were based on our previous work [38, 39] and the work of others [37, 40, 41].

Every neuron has sodium and potassium currents and the interaction between these currents results in different transitions between spiking and the silent state, therefore here we studied the effects of additional Na- and KM-channels on firing rates and DB of GCs. In the case of rather "weak" LFC cells with a small maximum firing rates and narrow domain of spiking, the additional Na- and KM-channels increased the firing rate and enlarged the domain so that it resembled the firing pattern of HFC cells. Interestingly, in the case of HFC cells addition of Na/KM channels had no effect on maximum firing rate with the exception of one neuron. Moreover, the addition of extra Na/KM channels has no influence on the initial transition to depolarization block, except for "flipping" cells.

The discovery of the "flipping" phenomenon is the major finding of this study. As we have metioned earlier (see Results) we defined "flipping" behavior as the ability of certain neurons to overcome the initial depolarization block in order to start generating trains of spikes at larger injected current steps before finally reaching another depolarization block. To the best of our knowledge, this neuronal behavior has not been previously reported in other experimental studies.

Importantly, we were able to reproduce "flipping" phenomenon in our computational model reaching the conclusion that, the appearance of "flipping" is linked to the number of states for the sodium channel of the model. The voltage-dependent sodium current was approximated by the 4-state Markov model from [28], and its reduction to the 3-state version. The 4-state model model describes two closed, one open and one inactivated states of the channel. This version of the model shows a sharp threshold over a 5 to 10 mV range, depending on the recent history of the channel, and the ability to recover from inactivation during repolarizations positive to earlier thresholds, without a large window current, therefore the available threshold depends on the history of firing, shifting down during the course of spike repolarization without giving a strong window current.

With three states for the Na channel, the model displays one periodic regime upon variations of the applied current, and this regime is bounded in parameter space by Hopf bifurcations. This scenario describes a typical non-flipping cell. However, when the number of states is increased to four a second periodic regime appears, bounded in parameter space by a second pair of Hopf bifurcations, at higher values of applied current. The two pairs of Hopf bifurcations are separated by a regime where the model admits a stable stationary state resembling an initial depolarization block. The presence of the second periodic regime arising at larger values of the input current is compatible with the "flipping" phenomenon, therefore we believe that the apperance of "flipping" it is due to the number of sodium channel states.

Heterogeneities in intrinsic excitability and firing patterns of granule cells have been frequently reported in the context of neurogenesis. As we previously described (see Introduction) the intrinsic firing properties and ionic conductances in GCs are thought to reflect their developmental stage and maturation. There is a general agreement that GCs expressing less mature phenotype, previously described by others as type-1 cells, are reaching a maximum number of spikes with current steps of moderate intensity. At current injections of high intensity, these cells are lacking sustained firing and are entering depolarization block. On the other hand GCs classified as type-2 are characterized by a linear firing in response to increasing current injections [30, 31]. It has been also recently reported that GCs located in different DG subregions exhibit different firing patterns [42]. Dentate gyrus, within each location along its dorso-ventral span, is anatomically segregated into three different sectors: the suprapyramidal blade, the crest region, and the infrapyramidal blade [43]. Across these sectors, granule cells manifest considerable heterogeneities in their intrinsic excitability, temporal summation, action potential characteristics, and frequency-dependent response properties. Having this in mind, the majority of our recordings were performed in the dorsal blade of the dentate gyrus within the crest. Therefore, it is not only possible, but more likely, that the two subpopulations of GCs described here (LFC vs HFC) are on a different stage of their maturation process, moreover we believe that the observed "flipping" phenomenon could be also correlated with neuronal maturation, especially when vast majority of "flipping" cells were LFC neurons. Immature neurons do not have a well-defined excitability identity (i.e. fixed conductivities) and rather have a fluid conductivity (akin to properties of stem cells) which enables them to explore the landscape of excitability types (1, 2 or 3). The final stage of maturation is stabilized via effectively being programmed by the environment set by local neuronal circuits in the DG.

We conjecture that our observed "flipping" behavior is induced by external electrical input (or in general electrical-chemical environment) that effectively pushes neurons to jump between classes of excitability. Without a proper "birth dating" technique (for example by using retroviral injections), that was not implemented here, unfortunately we cannot be sure. More research in the future will be required in order to describe "flipping" phenomenon in greater details and answer outstanding open questions: What is the possible role of "flipping"? Is "flipping" correlated with neuronal maturation? And finally, can this phenomenon be observed in other types of neurons in different brain regions?

Acknowledgments

We acknowledge support from Ikerbasque (The Basque Foundation for Science), the Basque Government through the BERC 2022-2025 program and by the Ministry of Science and Innovation: BCAM Severo Ochoa accreditation CEX2021-001142-S / MICIN / AEI / 10.13039/501100011033, Elkartek project "SiliconBurmuin" code KK-2023/00090, and the IKUR Strategy HPC-AI under the collaboration agreement

between Ikerbasque Foundation and BCAM on behalf of the Department of Education of the Basque Government

References

1. McCormick D, Contreras D. On the cellular and network bases of epileptic seizures. Annual Review of Physiology. 2001;63:815–846.
2. Dichter M, Ayala G. Cellular mechanisms of epilepsy — a status-report. Science. 1987;237:157–164.
3. Grace A, Bunney B, Moore H, Todd C. Dopamine-cell depolarization block as a model for the therapeutic actions of antipsychotic drugs. Trends in Neuroscience. 1997;20:31–37.
4. Bianchi D, Marasco A, Limongiello A, Marchetti C, Marie H, Tirozzi B, et al. On the mechanisms underlying the depolarization block in the spiking dynamics of CA1 pyramidal neurons. Journal of Computational Neuroscience. 2012;33:207–225.
5. Kuznetsova A, Huertas M, Kuznetsov A, Paladini C, Canavier C. Regulation of firing frequency in a computational model of a midbrain dopaminergic neuron. Journal of Computational Neuroscience. 2010;28:389–403.
6. Tucker KR, Huertas MA, Horn JP, Canavier CC, Levitan ES. Pacemaker rate and depolarization block in nigral dopamine neurons: a somatic sodium channel balancing act. Journal of Neuroscience. 2012;32(42):14519–14531.
7. Qian K, Yu N, Tucker KR, Levitan ES, Canavier CC. Mathematical analysis of depolarization block mediated by slow inactivation of fast sodium channels in midbrain dopamine neurons. Journal of neurophysiology. 2014;.
8. Economo MN, Fernandez FR, White JA. Dynamic clamp: alteration of response properties and creation of virtual realities in neurophysiology. Journal of Neuroscience. 2010;30(7):2407–2413.
9. Espósito MS, Piatti VC, Laplagne DA, Morgenstern NA, Ferrari CC, Pitossi FJ, et al. Neuronal differentiation in the adult hippocampus recapitulates embryonic development. Journal of Neuroscience. 2005;25(44):10074–10086.
10. Ge S, Goh EL, Sailor KA, Kitabatake Y, Ming Gl, Song H. GABA regulates synaptic integration of newly generated neurons in the adult brain. Nature. 2006;439(7076):589–593.
11. Toni N, Laplagne DA, Zhao C, Lombardi G, Ribak CE, Gage FH, et al. Neurons born in the adult dentate gyrus form functional synapses with target cells. Nature neuroscience. 2008;11(8):901–907.
12. Dieni CV, Nietz AK, Panichi R, Wadiche JI, Overstreet-Wadiche L. Distinct determinants of sparse activation during granule cell maturation. Journal of Neuroscience. 2013;33(49):19131–19142.
13. Wadiche LO, Bromberg DA, Bensen AL, Westbrook GL. GABAergic signaling to newborn neurons in dentate gyrus. Journal of neurophysiology. 2005;94(6):4528–4532.

14. Tozuka Y, Fukuda S, Namba T, Seki T, Hisatsune T. GABAergic excitation promotes neuronal differentiation in adult hippocampal progenitor cells. Neuron. 2005;47(6):803–815.

15. Bielefeld P, Durá I, Danielewicz J, Lucassen P, Baekelandt V, Abrous D, et al. Insult-induced aberrant hippocampal neurogenesis: Functional consequences and possible therapeutic strategies. Behavioural Brain Research. 2019;372:112032.

16. Hüttmann K, Sadgrove M, Wallraff A, Hinterkeuser S, Kirchhoff F, Steinhäuser C, et al. Seizures preferentially stimulate proliferation of radial glia-like astrocytes in the adult dentate gyrus: functional and immunocytochemical analysis. European Journal of Neuroscience. 2003;18(10):2769–2778.

17. Indulekha CL, Sanalkumar R, Thekkuveettil A, James J. Seizure induces activation of multiple subtypes of neural progenitors and growth factors in hippocampus with neuronal maturation confined to dentate gyrus. Biochemical and biophysical research communications. 2010;393(4):864–871.

18. Schmidt-Hieber C, Jonas P, Bischofberger J. Enhanced synaptic plasticity in newly generated granule cells of the adult hippocampus. Nature. 2004;429(6988):184–187.

19. Ge S, Pradhan DA, Ming Gl, Song H. GABA sets the tempo for activity-dependent adult neurogenesis. Trends in neurosciences. 2007;30(1):1–8.

20. Aimone JB, Deng W, Gage FH. Resolving new memories: a critical look at the dentate gyrus, adult neurogenesis, and pattern separation. Neuron. 2011;70(4):589–596.

21. Marín-Burgin A, Mongiat LA, Pardi MB, Schinder AF. Unique processing during a period of high excitation/inhibition balance in adult-born neurons. Science. 2012;335(6073):1238–1242.

22. Brunner J, Neubrandt M, Van-Weert S, Andrási T, Borgmann FBK, Jessberger S, et al. Adult-born granule cells mature through two functionally distinct states. Elife. 2014;3:e03104.

23. Dieni CV, Panichi R, Aimone JB, Kuo CT, Wadiche JI, Overstreet-Wadiche L. Low excitatory innervation balances high intrinsic excitability of immature dentate neurons. Nature communications. 2016;7(1):1–13.

24. Mongiat LA, Espósito MS, Lombardi G, Schinder AF. Reliable activation of immature neurons in the adult hippocampus. PloS one. 2009;4(4):e5320.

25. Van Praag H, Schinder AF, Christie BR, Toni N, Palmer TD, Gage FH. Functional neurogenesis in the adult hippocampus. Nature. 2002;415(6875):1030–1034.

26. Parent JM, Timothy WY, Leibowitz RT, Geschwind DH, Sloviter RS, Lowenstein DH. Dentate granule cell neurogenesis is increased by seizures and contributes to aberrant network reorganization in the adult rat hippocampus. Journal of Neuroscience. 1997;17(10):3727–3738.

27. Desroches M, Rinzel J, Rodrigues S. Classification of bursting patterns: A tale of two ducks. PLoS computational biology. 2022;18(2):e1009752.

28. Borg-Graham LJ. In: Ulinski PS, Jones EG, Peters A, editors. Interpretations of Data and Mechanisms for Hippocampal Pyramidal Cell Models. Boston, MA: Springer US; 1999. p. 19–138. Available from: https://doi.org/10.1007/978-1-4615-4903-1_2.

29. Jiang N, Cupolillo D, Grosjean N, Muller E, Deforges S, et al. Impaired plasticity of intrinsic excitability in the dentate gyrus alters spike transfer in a mouse model of Alzheimer's disease. Neurobiology of Disease. 2021;154:105345.

30. Ambrogini P, Lattanzi D, Ciuffoli S, Agostini D, Bertini L, Stocchi V, et al. Morpho-functional characterization of neuronal cells at different stages of maturation in granule cell layer of adult rat dentate gyrus. Brain research. 2004;1017(1-2):21–31.

31. Nenov MN, Laezza F, Haidacher SJ, Zhao Y, Sadygov RG, Starkey JM, et al. Cognitive enhancing treatment with a PPARγ agonist normalizes dentate granule cell presynaptic function in Tg2576 APP mice. Journal of Neuroscience. 2014;34(3):1028–1036.

32. Monier C, Chavane F, Baudot P, Graham LJ, Fregnac Y. Orientation and direction selectivity of synaptic inputs in visual cortical neurons: a diversity of combinations produces spike tuning. Neuron. 2003;37(4):663–680. doi:10.1016/s0896-6273(03)00064-3.

33. Chizhov AV, Graham LJ. A strategy for mapping biophysical to abstract neuronal network models applied to primary visual cortex. PLoS Comput Biol. 2021;17(8):e1009007. doi:10.1371/journal.pcbi.1009007.

34. Pokrovskii AN. Effect of synapse conductivity on spike development. Biofizika. 1978;23(4):649—-653.

35. Shriki O, Hansel D, Sompolinsky H. Rate models for conductance-based cortical neuronal networks. Neural computation. 2003;15(8):1809–1841.

36. Destexhe A, Bal T, editors. Dynamic-clamp: From principles to applications. New York: Springer; 2009.

37. Graham LJ, Schramm A. In Vivo Dynamic-Clamp Manipulation of Extrinsic and Intrinsic Conductances: Functional Roles of Shunting Inhibition and IBK in Rat and Cat Cortex. In: Bal T, Destexhe A, editors. Dynamic-clamp: From principles to applications. New York: Springer; 2009.

38. Chizhov AV, Malinina E, Druzin M, Graham LJ, Johansson S. Firing clamp: a novel method for single-trial estimation of excitatory and inhibitory synaptic neuronal conductances. Frontiers in cellular neuroscience. 2014;8:86. doi:10.3389/fncel.2014.00086.

39. Smirnova EY, Zaitsev AV, Kim KK, Chizhov AV. The domain of neuronal firing on a plane of input current and conductance. J Comput Neurosci. 2015;39(2):217–233. doi:10.1007/s10827-015-0573-5.

40. Fernandez FR, White JA. Reduction of spike afterdepolarization by increased leak conductance alters interspike interval variability. The Journal of Neuroscience: The Official Journal of the Society for Neuroscience. 2009;29(4):973–986. doi:10.1523/JNEUROSCI.4195-08.2009.

41. Fernandez FR, White JA. Gain control in CA1 pyramidal cells using changes in somatic conductance. The Journal of Neuroscience: The Official Journal of the Society for Neuroscience. 2010;30(1):230–241. doi:10.1523/JNEUROSCI.3995-09.2010.

42. Mishra P, Narayanan R. Heterogeneities in intrinsic excitability and frequency-dependent response properties of granule cells across the blades of the rat dentate gyrus. Journal of Neurophysiology. 2020;123(2):755–772.

43. Amaral DG, Scharfman HE, Lavenex P. The dentate gyrus: fundamental neuroanatomical organization (dentate gyrus for dummies). Progress in Brain Research. 2007;163:3–22.